Electronic Supplementary Material (ESI) for Chemical Communications
This journal is © The Royal Society of Chemistry 2011

## Supporting information for

# The rational synthesize of (10,3)-type MOFs based on tetraunclear $[W(Mo)OS_3Cu_3]^+$ secondary building units

**Xiao-Qiang Yao,[a] Zhao-Rui Pan,[a] Jin-Song Hu,[a] Yi-Zhi Li,[a] Zi-Jian Guo[a] and He-Gen Zheng*[ab]**

[a] *State Key Laboratory of Coordination Chemistry, School of Chemistry and Chemical Engineering, Nanjing National Laboratory of Microstructures, Nanjing University, Nanjing 210093, P. R. China.*

[b] *State Key Laboratory of Structural Chemistry, Fujian Institute of Research on the Structure of Matter, Chinese Academy of Sciences, Fuzhou 350002, P. R. China*

Fax: (+86)25-83314502, E-mail: zhenghg@nju.edu.cn

## Experimental Details

**Synthesis of $\{[MoOS_3Cu_3(bibp)_{2.5}](I)\}_n$ (1).** A well-ground mixture of $[NH_4]_2[MoO_2S_2]$ (0.114 g 0.5 mmol), CuI (0.382 g 2.0 mmol) and $Et_4NI$ (0.085 g 0.5 mmol) was firmly ground in an agate mortar, and firmly ground at room temperature for 30 min. During this time, the mixture became slightly moistened and then was extracted by DMF and $CH_3CN$ (5 ml; v/v 2:1) to get the dark red filtrate. bibp (0.143 g 0.5mmol) was added in the filtrate and the final mixture was sealed in a 15 ml PTFE-lined stainless-steel acid digestion bomb and heated at 100 °C for 2 days. Dark red prism-shaped single crystals suitable for X-ray diffraction were obtained in 12% yield, which were collected by filtration and washed with *i*-PrOH/$Et_2O$ (v/v; 1:2). Elemental and ICP analysis calcd (%) for ($MoOS_3Cu_3N_{10}C_{45}H_{35}I$): C 43.54, H 2.84, N 11.28. Cu 15.36, Mo 7.73; found: C 43.39, H 2.91, N 10.92. Cu 15.80, Mo 8.20; IR (KBr, $cm^{-1}$): 3476(m), 3417(s), 1637(m), 1618(s), 1508(m),

1457(m), 1384(m)，1303(w), 1248(w), 1092(m), 991(w), 822(w), 621(m), 483(w).

**Synthesis of {[$WOS_3Cu_3Br(TIPA)](H_2O)(DMF)$}$_n$ (2).** A well-ground mixture of $[NH_4]_2[WO_2S_2]$ (0.174g, 0.5 mmol), CuBr (0.282g, 1 mmol), $Et_4NBr$ (0.06 g, 0.5 mmol) was added to a mixture of DMF and $CH_3CN$ (15 mL; v/v 2:1) under a purified nitrogen atmosphere. After stirring for 10 h, tipa (0.221 g, 0.5 mmol) was added and the mixture was stirred for another 2h. And the final mixture was sealed in a 15 mL PTFE-lined stainless-steel acid digestion bomb and heated at 90 °C for 2 days. Light yellow hexagonal prism-shaped crystals suitable for X-ray diffraction were obtained in 13% yield, which were collected by filtration and washed with *i*-PrOH/$Et_2O$ (v/v; 1: 2). Elemental and ICP analysis calcd (%) for ($WS_3Cu_3BrC_{30}H_{30}O_3N_8$): C 32.72, H 2.75, N 10.18. Cu 17.31, W 16.69; found: C 32.18, H 2.31, N 11.32. Cu 17.80, W 17.10; IR (KBr, $cm^{-1}$): 3418(s), 1638(s), 1618(m), 1517(m), 1384(m), 1307(w), 1283(w), 1259(m), 1062(m), 931(w), 832(w), 621(m), 547(w).

**Physical Measurements**

X-ray crystallographic data of **1** and **2** were collected on a Bruker Apex Smart CCD diffractometer with graphite-monochromated Mo-Kα radiation (λ = 0.71073 Å).The structures were solved by direct methods, and the non-hydrogen atoms were located from the trial structure and then refined anisotropically with SHELXTL using full-matrix least-squares procedures based on $F^2$ values using the SHELXTL (version 6.10) package of crystallographic software. The hydrogen atom positions were fixed geometrically at calculated distances and allowed to ride on the parent atoms.

The IR absorption spectra were obtained in the range of 400-4000 $cm^{-1}$ by means of a Nicolet (Impact 410) spectrometer with KBr pellets.

Elemental analyses were performed on a Perkin-Elmer model 240C analyzer.

Inductively coupled plasma (ICP) analysis was carried out on a Perkin–Elmer Optima 3300DV

spectrometer

Thermo-gravimetric analysis (TGA) data were recorded by a simultaneous SDT 2960 thermal analyzer from 25 °C to 750 °C with a heating rate of 10 °C $min^{-1}$ in $N_2$ atmosphere (a flow rate of 100 mL $min^{-1}$).

X-ray diffraction (XRD) measurements were performed on a Bruker D8 Advance X-ray diffractometer using Cu Kα radiation (0.15418 nm), in which the X-ray tube was operated at 40 kV and 40 mA.

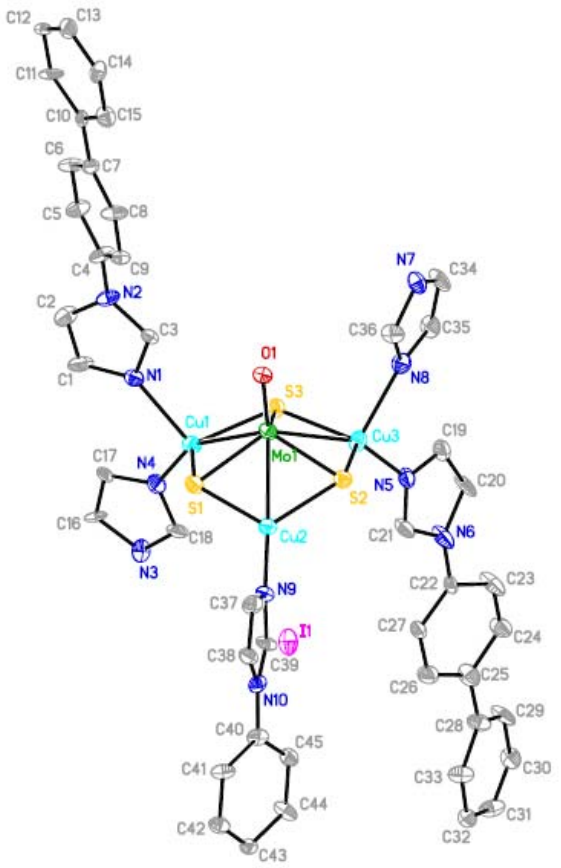


**Fig. S1** Plot of the asymmetric unit in **1** showing 30% ellipsoid probability (hydrogen atoms and water molecules are omitted for clarity) with labeling scheme.

This journal is © The Royal Society of Chemistry 2011

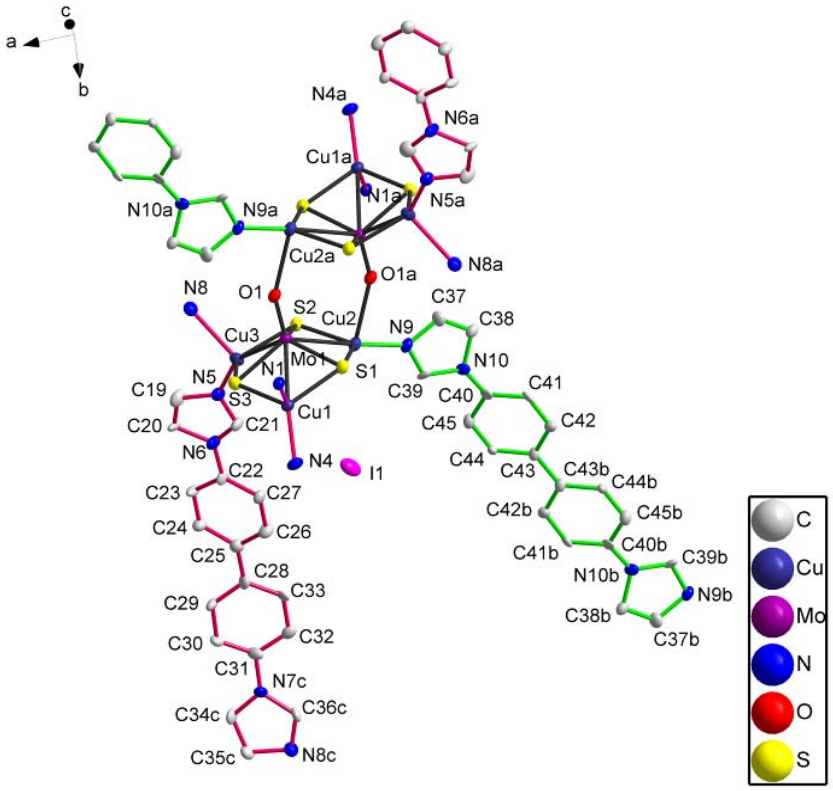


**Fig. S2** Coordination environment of **1** with 30% ellipsoid probability (hydrogen atoms and water molecules are omitted for clarity). Symmetry code: *a* = 1 - *x*, - *y*, 1 - *z*; b = - *x*, 1 - *y*, - *z*; c = *x*, 1 + *y*, - 1 + *z*.

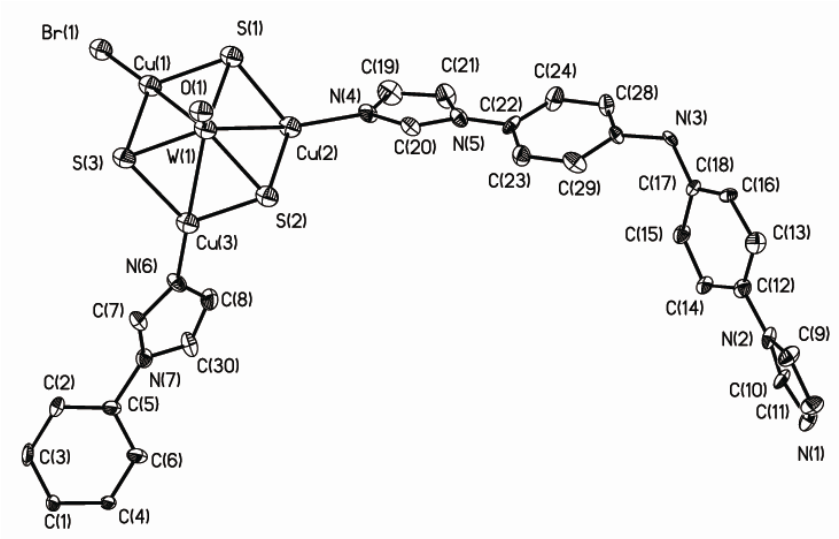


**Fig. S3** Plot of the asymmetric unit in **2** showing 30% ellipsoid probability (hydrogen atoms and water molecules are omitted for clarity) with labeling scheme.

This journal is © The Royal Society of Chemistry 2011

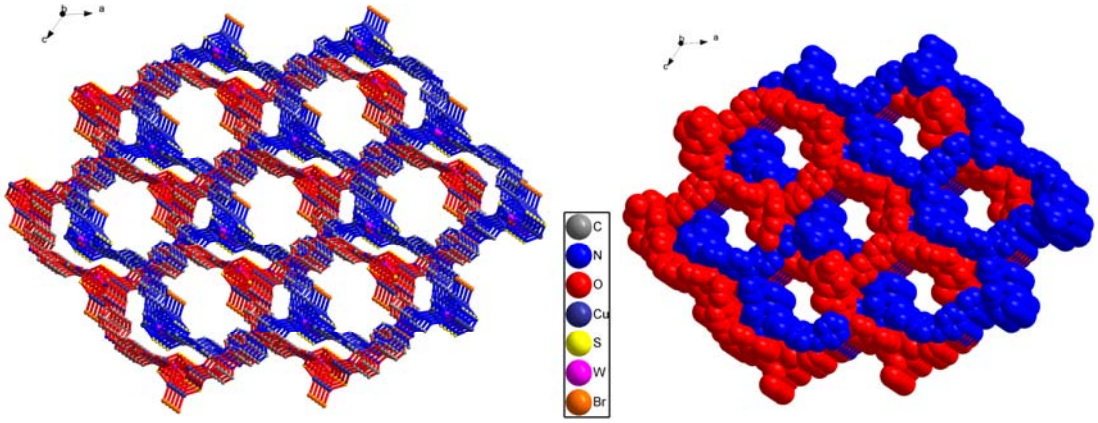


**Fig. S4** (Left) Portion of the 2-fold interpenetrated structure of **2**. (Right) The space-filling picture of **2**.

**Optical Measurement**

A modified Z-scan technique: top-hat Z-scan experiments have been performed on clusters **1** and **2** in N,N′-dimethyl formamide (DMF) solutions. The clusters are relatively stable toward air and laser light under the experimental conditions. The DMF solutions of **1** and **2** were placed in a 2 mm cuvette for NLO measurements. The nonlinear absorption and refraction were investigated with a linearly polarized laser light ($\lambda$ = 532 nm; pulse widths = 6.5 ns; repetition rate = 10 Hz) provided by a frequency-doubled, mode-locked, Q-switched Nd:YAG laser. The spatial profiles of the laser beam were nearly Top-hat distribution after passing through a spatial filter. The laser beam was focused with a 395 mm focal length focusing Lens. The radius of the beam waist was about 31 μm. The incident and transmitted pulse energies were measured simultaneously by two energy detectors (Laser Precision Rjp-765), which were linked to a computer via GPIB interface. The NLO properties of the samples were manifested by moving the samples along the axis of the incident laser irradiance beam (*z*-direction). The normalized closed-aperture curves are obtained by dividing the closed-aperture curve to the open-aperture one. In the far field, an aperture with linear transmittance of S = 5% was placed in front of the detector D2 to measure the transmitted energy when the assessment of laser beam distortion was needed.

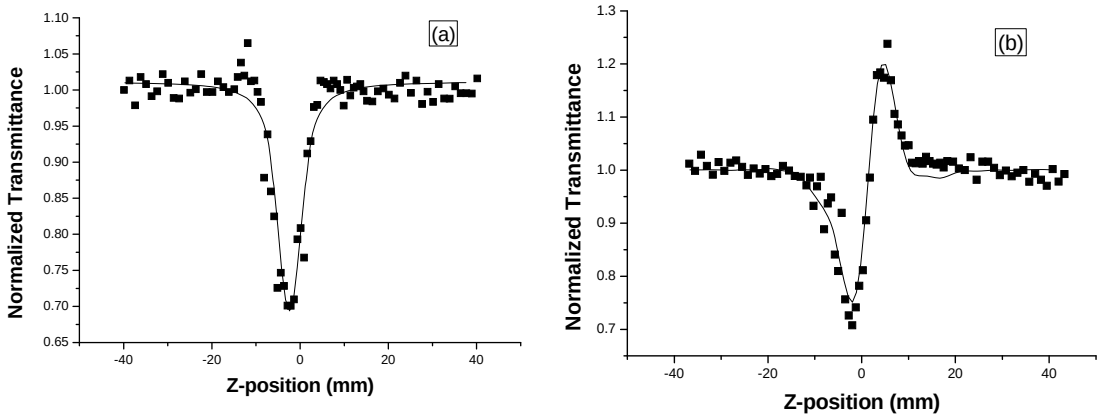


**Fig. S5** top-hat Z-scan measurement of **1** in $1.6\times10^{-4}$ mol $dm^{-3}$ DMF solution at 532 nm, 6.5 ns laser pulses, with a linear transmittance of 81%. The dark square represent the Z-scan experimental data and the solid lines are the theoretical fitting curves. (a) Data collected under the open-aperture configuration. (b) Data obtained by dividing the normalized Z-scan data obtained under the closed-aperture configuration by the normalized Z-scan data in (a).

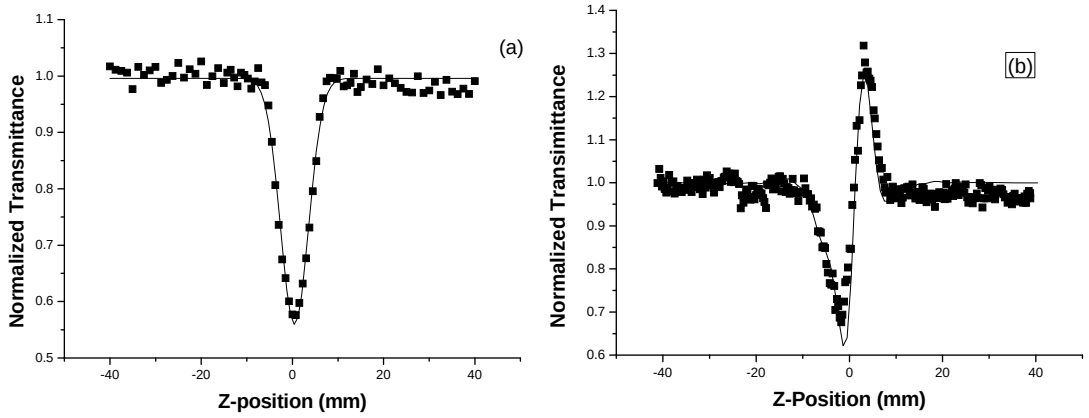


**Fig. S6** top-hat Z-scan measurement of **2** in $2.4\times10^{-4}$ mol $dm^{-3}$ DMF solution at 532 nm, 6.5 ns laser pulses, with a linear transmittance of 84%. The dark square represent the Z-scan experimental data and the solid lines are the theoretical fitting curves. (a) Data collected under the open-aperture configuration. (b) Data obtained by dividing the normalized Z-scan data obtained under the closed-aperture configuration by the normalized Z-scan data in (a).

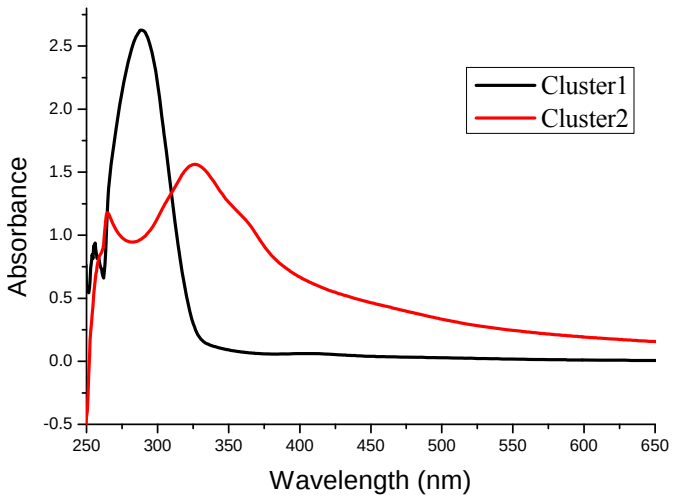


**Fig. S7** Electronic spectra of **1** and **2** ($1\times10^{-4}$ M) in DMF in a 1 cm thick glass cell.

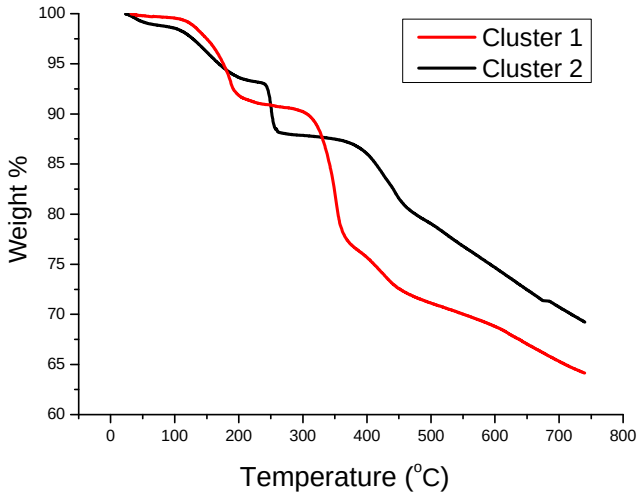


**Fig. S8** TGA plots of **1** and **2.**

The thermogravimetric analysis (TGA) was performed in $N_2$ atmosphere on polycrystalline samples of cluster **1** and **2**, and the TG curves are shown in Fig. S8. For **1**, the framework remains intact up to 110 °C, from which its framework begin to decompose. For **2**, the weight loss of 8.12% in the region of 23–240 °C corresponds to the loss of water and DMF molecules (8.27% calcd), whereupon the framework begins to collapse.

This journal is © The Royal Society of Chemistry 2011

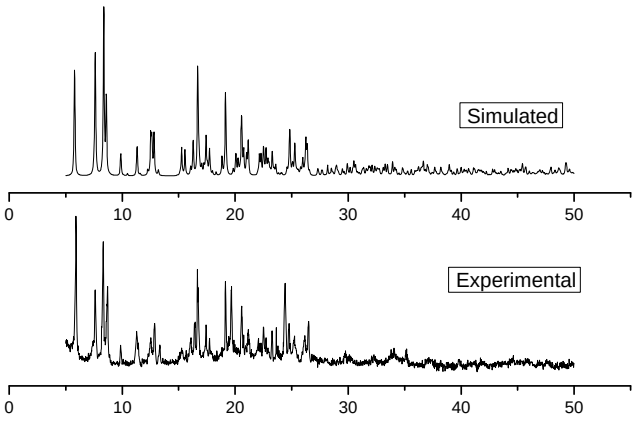


**Fig. S9** Experimental (bottom) and simulated (top) powder X-ray diffraction patterns of **1** at 293K.

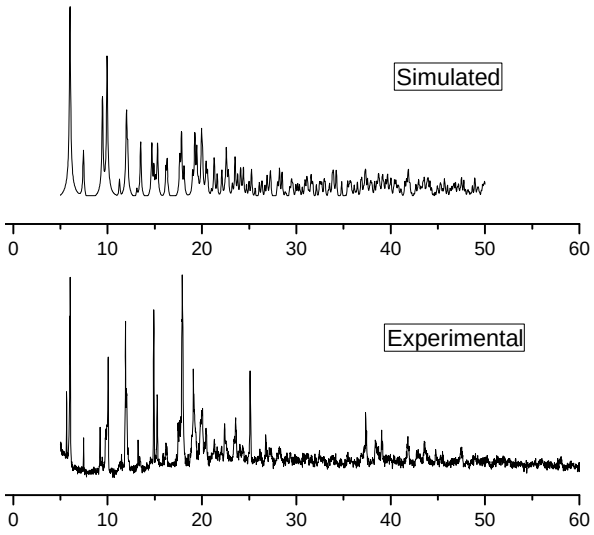


**Fig. S10** Experimental (bottom) and simulated (top) powder X-ray diffraction patterns of **2** at 293K.

This journal is © The Royal Society of Chemistry 2011

**Table S1 Selected Bond Distances (Å) and Angles (deg) for complexes**

| | | | |
|---|---|---|---|
| Complex **1** | | | |
| Mo(1)-O(1) | 1.707(4) | Cu(1)-Mo(1) | 2.6608(14) |
| Cu(2)-Mo(1) | 2.6167(13) | Cu(3)-Mo(1) | 2.6500(12) |
| Mo(1)-S(1) | 2.2602(18) | Mo(1)-S(2) | 2.2813(19) |
| Mo(1)-S(3) | 2.2517(19) | Cu(1)-S(1) | 2.300(2) |
| Cu(1)-S(3) | 2.2894(19) | Cu(1)-N(1) | 2.221(6) |
| Cu(1)-N(4) | 1.980(5) | Cu(2)-S(1) | 2.270(2) |
| Cu(2)-S(2) | 2.2520(18) | Cu(2)-N(9) | 1.911(5) |
| Cu(2)-O(1)_*a* | 2.406(5) | O(1)-Cu(2)_*a* | 2.406(5) |
| Cu(3)-S(2) | 2.289(2) | Cu(3)-S(3) | 2.3133(19) |
| Cu(3)-N(5) | 1.990(5) | Cu(3)-N(8) | 2.273(6) |
| N(4)-Cu(1)-N(1) | 103.0(2) | N(4)-Cu(1)-S(3) | 118.69(18) |
| N(1)-Cu(1)-S(3) | 108.49(14) | N(4)-Cu(1)-S(1) | 119.15(19) |
| N(1)-Cu(1)-S(1) | 99.66(15) | S(3)-Cu(1)-S(1) | 105.68(7) |
| N(9)-Cu(2)-S(2) | 126.39(17) | N(9)-Cu(2)-S(1) | 124.24(16) |
| S(2)-Cu(2)-S(1) | 109.26(7) | N(9)-Cu(2)-O(1)_*a* | 88.0(2) |
| S(2)-Cu(2)-O(1)_*a* | 92.84(12) | S(1)-Cu(2)-O(1)_*a* | 93.01(12) |
| N(5)-Cu(3)-N(8) | 104.8(2) | N(5)-Cu(3)-S(2) | 119.69(18) |
| N(8)-Cu(3)-S(2) | 102.09(16) | N(5)-Cu(3)-S(3) | 118.95(17) |
| N(8)-Cu(3)-S(3) | 101.41(16) | S(2)-Cu(3)-S(3) | 106.79(7) |
| O(1)-Mo(1)-S(3) | 111.09(16) | O(1)-Mo(1)-S(1) | 110.35(16) |
| S(3)-Mo(1)-S(1) | 108.32(7) | O(1)-Mo(1)-S(2) | 109.30(16) |
| S(3)-Mo(1)-S(2) | 109.18(7) | S(1)-Mo(1)-S(2) | 108.55(7) |
| Symmetric codes: *a* = - *x* + 1, - *y*, - *z* + 1 | | | |
| Complex **2** | | | |
| W(1)-O(1) | 1.703(5) | W(1)-S(1) | 2.2632(19) |
| W(1)-S(2) | 2.259(2) | W(1)-S(3) | 2.255(2) |
| W(1)-Cu(1) | 2.6381(11) | W(1)-Cu(2) | 2.6907(9) |
| W(1)-Cu(3) | 2.6453(9) | Cu(1)-S(3) | 2.245(2) |
| Cu(1)-Br(1) | 2.2613(13) | Cu(2)-S(2) | 2.284(2) |
| Cu(2)-S(1) | 2.290(2) | Cu(2)-N(1)_*b* | 2.094(5) |
| Cu(2)-N(1)_*a* | 2.094(5) | Cu(3)-S(2) | 2.260(2) |
| Cu(3)-S(3) | 2.274(2) | Cu(3)-N(6) | 1.932(5) |
| O(1)-W(1)-S(2) | 110.33(19) | O(1)-W(1)-S(3) | 110.92(18) |
| S(1)-Cu(1)-Br(1) | 126.89(7) | O(1)-W(1)-S(1) | 110.73(17) |
| S(2)-W(1)-S(1) | 108.12(7) | S(2)-Cu(2)-S(1) | 106.35(8) |
| S(3)-Cu(1)-Br(1) | 124.40(7) | S(2)-Cu(3)-S(3) | 107.88(8) |
| S(3)-Cu(1)-S(1) | 108.71(8) | S(3)-W(1)-S(2) | 108.62(7) |
| S(3)-W(1)-S(1) | 108.03(8) | N(4)-Cu(2)-S(2) | 117.44(19) |
| N(1)_*a*-Cu(2)-S(2) | 110.95(17) | N(4)-Cu(2)-S(1) | 120.80(18) |
| N(1)_*a*-Cu(2)-S(1) | 105.74(17) | N(4)-Cu(2)-N(1)_*a* | 94.1(2) |
| N(6)-Cu(3)-S(2) | 127.09(19) | N(6)-Cu(3)-S(3) | 124.1(2) |
| Symmetric codes: *a* = *x*, - *y* + 2, *z* + 1/2; *b* = *x*, - *y* + 2, *z* - 1/2 | | | |